Available online at www.sciencedirect.com
SCIENCE DIRECT®
International Journal of Heat and Mass Transfer 48 (2005) 3308–3318
International Journal of HEAT and MASS TRANSFER
www.elsevier.com/locate/ijhmt

A numerical study of natural convection in a horizontal enclosure with a conducting body

Jae Ryong Lee, Man Yeong Ha *

School of Mechanical Engineering, Pusan National University, San 30, Chang Jeon Dong, Kum Jeong Gu, Pusan 609-735, Republic of Korea

Received 12 August 2004; received in revised form 25 February 2005
Available online 19 April 2005

Abstract

The physical model considered here is a horizontal layer of fluid heated below and cold above with a conducting body placed at the center of the layer. The body has dimensionless thermal conductivities of 0.1, 1 and 50. Two-dimensional solution for unsteady natural convection is obtained using an accurate and efficient Chebyshev spectral methodology for different Rayleigh numbers. Multi-domain technique is used to handle a square-shaped conducting body. The results for the case of a conducting body are also compared to those of adiabatic and neutral isothermal bodies. When the dimensionless thermal conductivity is 0.1, a pattern of fluid flow and isotherms and the corresponding surface- and time-averaged Nusselt number are almost the same as the case of an adiabatic body. When the dimensionless thermal conductivity is 50, a pattern of flow and isotherm and the corresponding surface- and time-averaged Nusselt number are similar to those of neutral isothermal body. The results for the case of dimensionless thermal conductivity of unity are also compared to those of pure natural convection.

1. Introduction

Rayleigh–Bénard convection in a horizontal layer of fluid confined between two parallel plates, with the bottom plate heated and the top one cooled, has been well studied for over a century. It has been well established that for the isothermal boundary condition the horizontal layer of fluid becomes unstable above a Rayleigh number of 1708 and convective motion sets in the form of steady convective rolls of aspect ratio (width to height) of about 2 [1]. With increasing Rayleigh number the flow undergoes a sequence of instabilities and eventually transitions to a turbulent state above a Rayleigh number of about 10^7 [2,3].

For couples of decades, there have been many researches about vertical cavity with two vertical walls at different temperatures and with adiabatic horizontal surfaces [4–6]. Natural convection flows in a vertical cavity are probably the most considered configuration in the studies of natural convection because of their relative simplicity and practical importance. Two- and three-dimensional numerical analysis for a vertical cavity with and without a body at the center has been performed in the past over a wide range of Rayleigh numbers. These studies suggested a set of benchmark numerical results for the two- and three-dimensional laminar and turbulent flow for varying Rayleigh numbers.

* Corresponding author. Tel.: +82 51 510 2440; fax: +82 51 512 9835.
E-mail address: myha@pusan.ac.kr (M.Y. Ha).

0017-9310/$ - see front matter © 2005 Elsevier Ltd. All rights reserved.
doi:10.1016/j.ijheatmasstransfer.2005.02.026

Nomenclature

g	gravity
k	dimensionless thermal conductivity ($=k_s/k_f$)
L	length of the enclosure
$\mathbf{n}$	vector normal to surface
Nu	local Nusselt number
$\overline{Nu}$	surface-averaged Nusselt number
$\langle\overline{Nu}\rangle$	time- and surface-averaged Nusselt number
p	dimensionless pressure
Pr	Prandtl number
Ra	Rayleigh number
t	dimensionless time
t^*	dimensional time
t_p	period of time integration
$\mathbf{u}$	dimensionless velocity
$\mathbf{u}^*$	dimensional velocity
$\mathbf{x}$	dimensionless coordinate vector
$\mathbf{x}^*$	dimensional i-directional coordinate
α	dimensionless thermal diffusivity ($=\alpha_s/\alpha_f$)
β	thermal expansion coefficient
ν_f	kinematic viscosity of fluid
θ	dimensionless temperature

Subscripts/superscripts

body	body
c	cold
f	fluid
h	hot
p	period
s	solid

The geometries that arise in engineering applications, however, are more complicated than a simple horizontal or vertical cavity. Considerable research has been performed with various obstacles placed inside the enclosure in the form of partitions, partial baffles and square bodies. These researches revealed that these kinds of obstructions could change the characteristics of flow and heat transfer in the horizontal and vertical enclosures.

House et al. [7] numerically examined the effect of a centered, squared heat-conducting body on the steady natural convection in a vertical square enclosure. They found that heat transfer across the enclosure may be enhanced or decreased by a body with a thermal conductivity ratio less than or larger than unity. Oh et al. [8] and Ha et al. [9] investigated the steady and unsteady natural convection processes when a temperature difference exists across the vertical enclosure and, at the same time, a conducting body generates heat within the vertical enclosure. They investigated the effects of Rayleigh numbers and temperature difference ratios on the fluid flow and heat transfer in the vertical enclosure. Ha and Jung [10] conducted numerical simulation to investigate three-dimensional, steady, conjugate heat transfer of natural convection and conduction in a vertical cubic enclosure within which a centered, cubic, heat-conducting body generates heat.

Ha et al. [11] solved the problem of two-dimensional and unsteady natural convection in a horizontal square enclosure with a square body located at the center between the bottom hot and top cold walls. To see the effects of the presence of a body and its thermal boundary conditions on natural convection between the hot and cold walls, they considered the cases that the body maintains the adiabatic and isothermal thermal boundary conditions for different Rayleigh numbers. Lee et al. [12] studied thermal convection in a horizontal layer of fluid heated from below and cooled from above, with a periodic array of evenly spaced square cylinders occupying the layer (whose aspect ratio is 6). They concluded that the transition of flow from quasi-steady up to unsteady convection depended on the presence of bodies and aspect ratio effect of the cell.

However, there is little information about natural convection processes when a heat-conducting body exists within a horizontal layer of fluid confined between the bottom hot and top cold walls. In this situation, the flow and heat transfer inside the enclosure are largely affected by the thermal conductivity ratio between solid body and fluid layer for different Rayleigh numbers. The purpose of this study is to examine how the thermal conductivity ratio affects the unsteady natural convection phenomena for different Rayleigh numbers when a heat-conducting body exists in the horizontal enclosure. The present results are compared with pure Rayleigh–Bénard convection and with the cases when a square body in the enclosure is adiabatic and neutral [11], in order to see the effect of the conducting body on the fluid flow and heat transfer in the horizontal enclosure.

2. Numerical methodology

A schematic of the system considered in present paper is shown in Fig 1. The system consists of a square enclosure with sides of length L, within which another square body with sides of length W is centered. The bottom wall is kept at a constant high temperature of T_h, whereas the top wall is kept at a constant low temperature of T_c. The left and right side walls are assumed to be

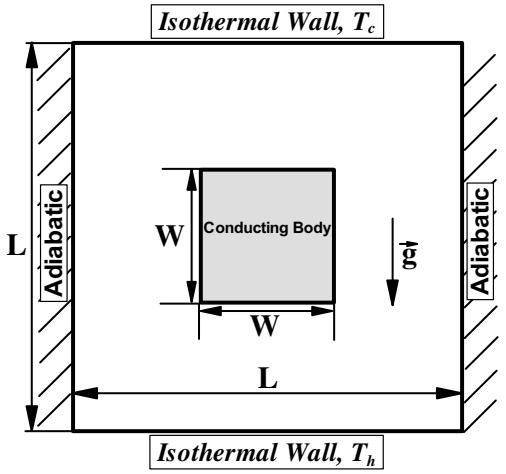

Fig. 1. A schematic of the system.

insulated. In this study, we assume that the radiation effects can be taken to be negligible. The fluid properties are also assumed to be constant, except for the density in the buoyancy term, which follows the Boussinesq approximation. The gravitational acceleration acts in the negative y-direction. Thus, in the present study, we observe the fluid flow and thermal fields for the natural convection in an enclosure with heat-generating conducting body at the center.

We solve the continuity, Navier–Stokes and energy equations in their non-dimensional forms defined as

$$\nabla \cdot \mathbf{u} = 0 \tag{1a}$$

$$\frac{\partial \mathbf{u}}{\partial t} + \mathbf{u} \cdot \nabla \mathbf{u} = -\nabla p + Pr\nabla^2 \mathbf{u} + Ra\,Pr\theta\,\mathbf{k}_2 \tag{1b}$$

$$\frac{\partial \theta_f}{\partial t} + \mathbf{u} \cdot \nabla \theta_f = \nabla^2 \theta_f \tag{1c}$$

$$\frac{\partial \theta_s}{\partial t} = \alpha \nabla^2 \theta_s \tag{1d}$$

The dimensionless variables in the above equations are defined as

$$t = \frac{t^* \alpha_f}{L^2}, \quad \mathbf{x} = \frac{\mathbf{x}^*}{L}, \quad \mathbf{u} = \frac{\mathbf{u}^* L}{\alpha_f},$$
$$P = \frac{P^* L^2}{\rho_f \alpha_f^2}, \quad \theta = \frac{T - T_c}{T_h - T_c}, \quad \alpha = \frac{\alpha_s}{\alpha_f} \tag{2}$$

In the above equations, ρ, T, α_s and α_f represent the density, dimensional temperature, thermal diffusivity of solid and fluid, respectively. The superscript $*$ in Eq. (2) represents the dimensional variables. u_i, p, t, θ and α are the non-dimensional velocity, pressure, time, temperature and thermal diffusivity. The above non-dimensionalization results in two dimensionless parameters: $Pr = \frac{\nu}{\alpha_f}$ and $Ra = \frac{g\beta L^3 (T_h - T_c)}{\nu \alpha_f}$ where ν, g and β are the kinematic viscosity, gravitational acceleration and volume expansion coefficient. In the simulations to be reported here the Prandtl number, Pr, has been taken to be 0.7 corresponding to that of air. The Rayleigh number, Ra, is varied over the range of 10^3–10^6.

For the boundary conditions, the velocities are set to zero for all solid walls. The temperature boundary conditions and the conditions at the fluid/body interfaces are as follows:

$$\text{At } x = 0 \quad \text{and} \quad 1; \quad \frac{\partial \theta}{\partial x} = 0$$
$$\text{At } y = 0; \quad \theta = 1$$
$$\text{At } y = 1; \quad \theta = 0$$
$$\text{At fluid/body interface;} \quad \theta_s = \theta \quad \text{and} \quad \frac{\partial \theta}{\partial \mathbf{n}} = k \frac{\partial \theta_s}{\partial \mathbf{n}}$$

where $k(=k_s/k_f)$ is a thermal conductivity ratio of conducting solid body to fluid and $\mathbf{n}$ is a vector normal to solid surface.

A spectral multi-domain methodology is used to perform the spatial discretization along the horizontal (x) and vertical (y) directions and to consider the heat-conducting square body at the center of computational domain [13]. In this technique the overall computational domain is subdivided into a number of smaller rectangular subdomains. Within each subdomain a local spectral Chebyshev discretization is defined [13]. Fig. 2 shows the computational geometry involving nine subdomains in the $x - y$ plane, with each subdomain resolved by up to 31×31 points. The grid points are the Gauss–Lobatto points corresponding to Chebyshev expansion within

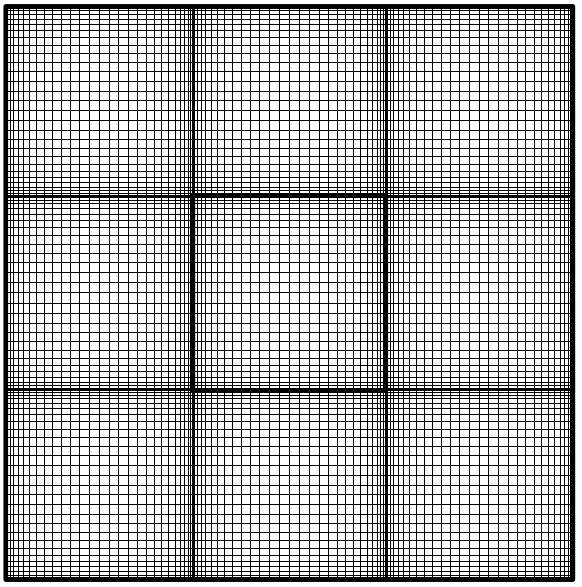

Fig. 2. Grid distribution of computational domain.

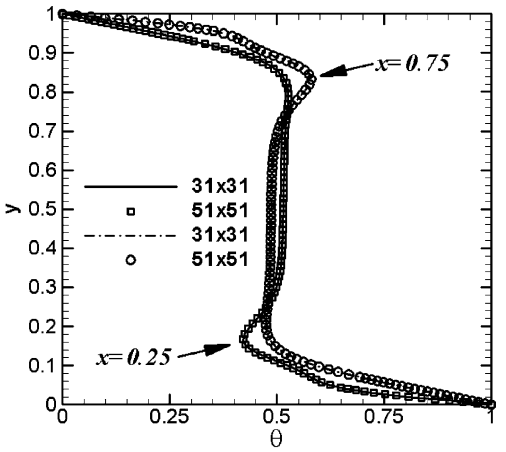

Fig. 3. Temperature profiles along the y direction at different locations of $x = 1/4$ and 3/4 for the coarse (31×31 in each subdoamin) and fine (51×51 in each subdomain) grid solutions.

each subdomain and are therefore non-uniformly distributed. Grid independence of the solution has been tested with additional simulations on much finer grids up to 51×51 points. Fig. 3 shows the temperature profiles along the y direction at different locations of $x = 1/4$ and 3/4 for the coarse (31×31 in each subdomain) and fine (51×51 in each subdomain) grid solutions when $Ra = 10^6$ and $k = 0.1$. The solutions using the coarse and find grids are almost the same. Thus the grid system of 31×31 points in each subdomain is adopted for the calculation of all the cases considered in the present study.

A two-step time-split scheme is used to advance the flow field [12]. First the velocity is advanced from time level 'n' to an intermediate level by solving the advection–diffusion equation. In the advection–diffusion step, the non-linear terms are treated explicitly using third-order Adams–Bashforth scheme. The diffusion terms are treated implicitly using Crank–Nicholson scheme. Then a Poisson equation for pressure is solved fully implicitly. The final divergence-free velocity field at '$n + 1$' is obtained with a pressure-correction step. After obtaining the velocity field, the temperature field is advanced in a similar manner with third-order Adams–Bashforth for the advection term and Crank–Nicholson scheme for the diffusion term. Once the velocity and temperature fields are obtained, the local, surface-averaged, time-averaged, and time- and surface-averaged Nusselt number are defined as

$$Nu = \left.\frac{\partial\theta}{\partial n}\right|_{\text{wall}}, \quad \overline{Nu} = \frac{1}{L}\int_0^L Nu\,\mathrm{d}S,$$
$$\langle Nu\rangle = \frac{1}{t_\mathrm{p}}\int_0^{t_\mathrm{p}} Nu\,\mathrm{d}t, \quad \langle\overline{Nu}\rangle = \frac{1}{t_\mathrm{p}}\int_0^{t_\mathrm{p}} \overline{Nu}\,\mathrm{d}t \tag{3}$$

where n is normal to the walls and t_p is the period of time integration. The above quantities are separately computed for the top cold and the bottom hot walls.

The present multi-domain spectral methodology and the computer code used here have been thoroughly validated by comparing results with those of de Vahl Davis [14], House et al. [7] and Le Quere [15] for the case of a vertical enclosure and with those of Lipps [2] for the case of a horizontal enclosure. For Rayleigh numbers 10^3, 10^4, 10^5 and 10^6 the benchmark results on surface-averaged Nusselt number obtained by de Vahl Davis [14] are 1.118, 2.243, 4.519 and 8.800. The corresponding results obtained with the present code using nine subdomains with 31×31 grid points resolving each subdomain are respectively, 1.118, 2.246, 4.525 and 8.821, yielding less than 0.25% difference, even at the highest Rayleigh number considered. The problem of natural convection in a vertical enclosure with an interior conducting body studied by House et al. [7] was also considered with the present code. The Nusselt number at the hot wall obtained by House et al. [7] for $Ra = 10^5$ with two different body-to-fluid thermal conductivity ratios of 0.2 and 5.0 are respectively, 4.324 and 4.624, for a dimensionless body size of 1/2. The corresponding results obtained with the present code using nine subdomains with 31×31 grid points resolving each subdomain are 4.324 and 4.631. Again the errors are less than 0.15%. Table 1 show the summary of these benchmark values.

3. Results and discussion

Fig. 4 shows isotherms and streamlines in the enclosure for different Rayleigh numbers with heat-conducting body at $k = 0.1$ and $\alpha = 0.001$. Fig. 4 also shows the results for the case when an adiabatic body is present at the center, in order to compare its results with the present ones. When $Ra = 10^3$, the heat transfer in the enclosure is predominantly due to conduction. When $k = 0.1$, the thermal conductivity of fluid is ten times larger than that of conducting body and as a result a heat-conducting body does not conduct well heat through the body. Thus a heat-conducting body at $k = 0.1$ acts like an adiabatic body and the distribution of isotherms at $k = 0.1$ and $Ra = 10^3$ is similar to that for the case of adiabatic body as shown in Fig. 4(a) and in the reference [11]. The isotherms are satisfied with a top–bottom reflectional symmetry about the horizontal midplane ($y = 1/2$) (see Eq. (4a)). Also along the horizontal direction reflectional symmetries can be observed about $x = 1/2$ (see Eq. (4b)).

Symmetry about $y = L/2$:

$$\{u', v', \theta', x', y'\} \leftarrow \{u, -v, (1-\theta), x, L-y\} \tag{4a}$$

Table 1
Comparison of the surface-averaged Nusselt number at the hot wall obtained from the present calculation with that from de Vahl Devis [14], House et al. [7] and Le Quere [15]

Ra	$\Gamma(=W/L)$	*k*	Surface-averaged Nusselt number at hot wall				
			Present study	de Vahl Devis [14]	House et al. [7]	Le Quere [15]	Error (%)
10^3	–	–	1.118	1.118	–	–	0
10^4	–	–	2.246	2.243	–	–	0.13
	–	–	4.525	4.519	–	–	0.13
10^5	0.5	5.0	4.324	–	4.324	–	0
	0.5	0.2	4.631	–	4.624	–	0.15
10^6	–	–	8.821	8.800	–	8.825	0.04
10^7	–	–	16.524	–	–	16.523	0.0006

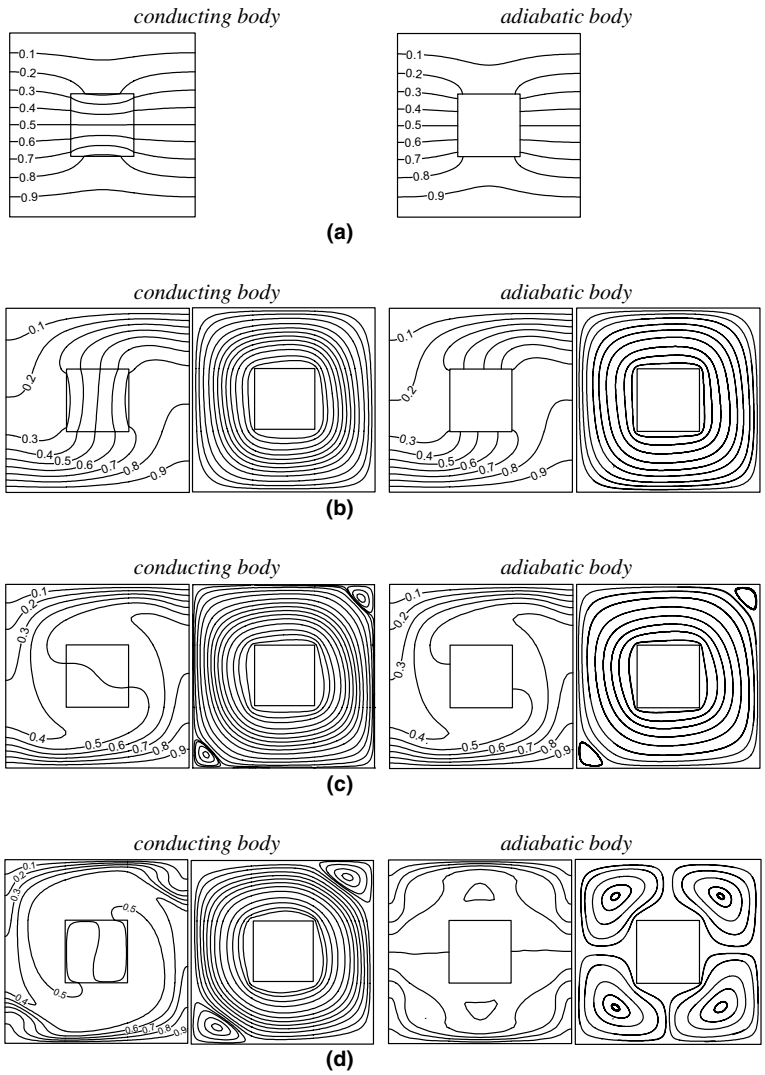

Fig. 4. Distribution of isotherms and streamline for the conducting body at $k = 0.1$ and $\alpha = 0.001$, and for the adiabatic body for different Rayleigh numbers: (a) $Ra = 10^3$; (b) $Ra = 10^4$; (c) $Ra = 10^5$; (d) $Ra = 10^6$.

Symmetry about $x = L/2$:

$$\{u', v', \theta', x', y'\} \leftarrow \{-u, v, \theta, L - x, y\} \tag{4b}$$

For the case of pure Rayleigh–Bénard convection without any bodies and obstacles in the enclosure, a convection caused by the buoyant force starts to occur in the form of steady roll when a Rayleigh number is larger than 1708 [1]. When $Ra = 10^4$, the fluid flow circulating in the counter-clockwise direction around a conducting body is formed in the enclosure and the corresponding isotherms also circulates in the counter-clockwise direction. The symmetric shapes about $x = 1/2$ and $y = 1/2$ of isotherms and streamlines are broken and changed them into diagonally symmetric ones.

If the Rayleigh number is increased to 10^5, the thickness of the thermal boundary layer formed on the top and bottom walls becomes thinner due to the flow acceleration and the gradient of thermal boundary layer becomes larger, meaning that the heat transfer rate increases with increasing Rayleigh number. We can also observe the formation of secondary vortices at the right top and left bottom corners of the enclosure. When $Ra \leqslant 10^5$ for $k = 0.1$, the fluid flow and isotherms reach a steady state after initial transients for both cases of conducting and adiabatic bodies. Thus the streamlines and isotherms shown in Fig. 4(a)–(c) show the fluid flow and temperature fields after they reach a steady state. The distribution of streamlines and isotherms formed in the enclosure for the case of conducting body is similar to that for the case of adiabatic body as shown in Fig. 4(a)–(c). Thus, when $Ra \leqslant 10^5$, the values of surface-averaged Nusselt number at the bottom hot wall for the case of conducting body are almost same as those for the case of adiabatic body as shown in Table 2.

When the Rayleigh number increases further to 10^6, the magnitude of velocity circulating in the counter-clockwise direction and the size of secondary vortices formed on the corners also increase further. When $Ra = 10^6$, the fluid flow and heat transfer in the enclosure for the case of conducting body are still steady like those when $Ra \leqslant 10^5$. However, the distribution of fluid flow and temperature fields for the case of adiabatic body is time-dependent in a periodically oscillatory fashion at the same Rayleigh number of 10^6 [12]. Thus, the streamlines and isotherms for the case of adiabatic body shown in Fig. 4(d) are time-averaged ones. In the presence of conducting body, there exists heat transfer between the conducting body and surrounding fluid, causing the flow and heat transfer more stable compared to the case of adiabatic body without any heat transfer between the body and surrounding fluid. Thus the streamlines and isotherms for the case of conducting body have different distribution compared to those for the case of adiabatic body as shown in Fig. 4(d). Due to this difference in the distribution of isotherms when $Ra = 10^6$, the value of surface- and time-averaged Nusselt number at the bottom hot wall for the case of conducting body has about 7% difference compared to that for the case of adiabatic body, unlike little difference when $Ra \leqslant 10^5$, as shown in Table 2. When the Rayleigh number is 10^4, 10^5 and 10^6 at $k = 0.1$, the streamlines and isotherms circulating in the counter-clockwise direction for the case of conducting body are diagonally symmetric and satisfy the following relation.

Table 2
Time- and surface-averaged Nusselt number on the hot wall

k	Ra			
	10^3	10^4	10^5	10^6
0.1	0.81	2.31	3.85	6.30
[Adiabatic [11]]	0.77	2.35	3.8	5.85
1	1.00	2.13	3.88	6.29
[Pure RB [11]]	1.00	2.16	3.91	6.30
50	1.27	1.56	3.94	6.31
[Neutral [11]]	1.29	1.50	3.90	6.19

Diagonal symmetry :

$$\{u', v', \theta', x', y'\} \leftarrow \{-u, -v, (1 - \theta), L - x, -y\} \tag{5}$$

If we call the solution shown in Fig. 4, $(\mathbf{u}_1, \theta_1)$, a new steady solution $(\mathbf{u}_2, \theta_2)$ can be obtained by enforcing one of the broken symmetries, say Eq. (4). Due to diagonal symmetry $(\mathbf{u}_2, \theta_2)$ will automatically satisfy Eq. (4) as well. Thus there are two stable fixed points and the phase space splits into two halves and, depending on where the flow starts, one or the other fixed point is reached. This alternate steady state solution corresponds to a large clockwise circulation around the body. Both of these two possible stable states are reached in any given simulation depending on the initial starting condition used in the time marching procedure.

Fig. 5 shows isotherms and streamlines in the enclosure for different Rayleigh numbers with heat-conducting body at $k = 50$ and $\alpha = 0.05$. Fig. 5 also shows the results for the case when a isothermal neutral body ($\theta = 0.5$) is present at the center, in order to compare its results with the present ones. When $k = 50$, a thermal conductivity of fluid is 50 times less than solid thermal conductivity. Because a heat-conducting body conducts well heat through the body, the temperature of conducting body is almost uniform and close to $\theta = 0.5$. Thus the flow and temperature fields for the case of $k = 50$ are generally similar to the case of neutral body.

As aforementioned, when $k = 0.1$, the thermal conductivity of conducting body is very smaller than the fluid. Thus the temperature in the conducting body is not uniform and has a large gradient. However, the temperature in the conducting body for the case of $k = 50$ is almost uniform due to large thermal conductivity of conducting body. As a result, when $Ra = 10^3$ and 10^4

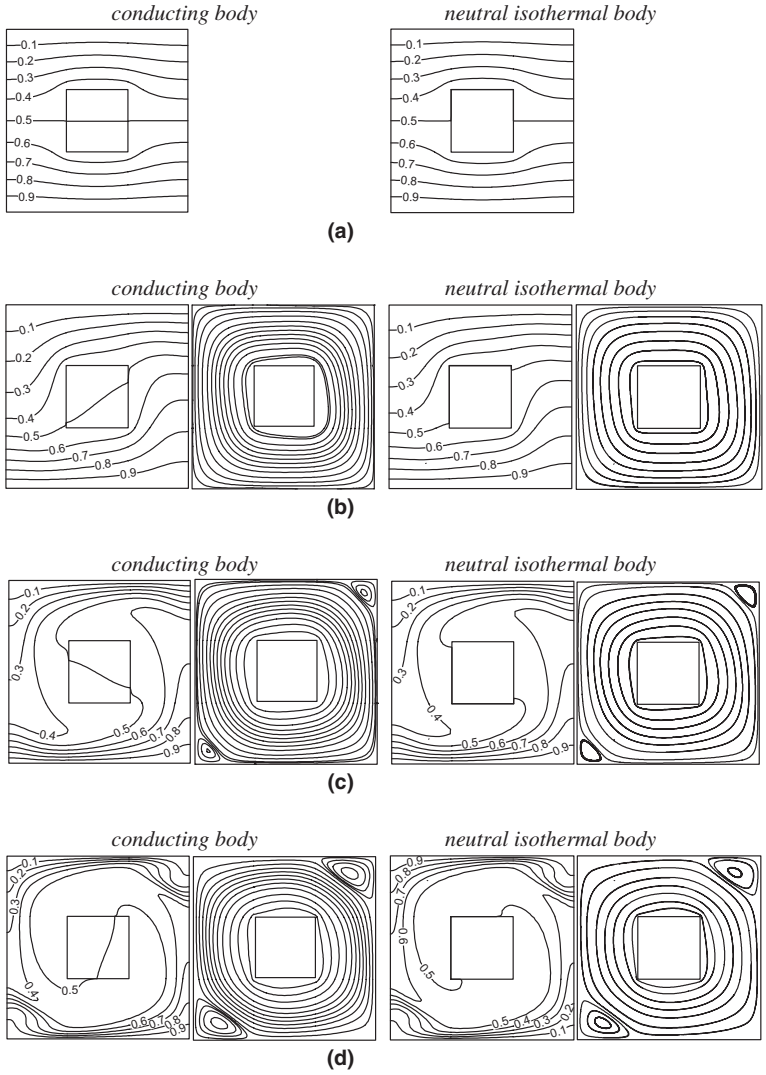

Fig. 5. Distribution of isotherms and streamline for the conducting body at $k = 50$ and $\alpha = 0.05$, and for the neutral isothermal body for different Rayleigh numbers: (a) $Ra = 10^3$; (b) $Ra = 10^4$; (c) $Ra = 10^5$; (d) $Ra = 10^6$.

at which conduction is more dominant heat transfer mode, the temperature fields for the case of $k = 50$ have different distribution from those for the case of $k = 0.1$. Especially differences in the inside of and around the conducting body are large. When the Rayleigh number increases to 10^5 and 10^6, the thermal resistance for conduction in the conducting body does not change but the thermal resistance for convection in the fluid decreases with increasing convective heat transfer. Thus, when $Ra = 10^5$ and 10^6, the distribution of isotherms for $k = 50$ is similar to that for $k = 0.1$, except for the slight difference in and close to the conducting body. The flow fields for the case of $k = 50$ are generally similar to those for the cases of $k = 0.1$ and neutral body. The flow in the enclosure circulates in the counter-clockwise direction. The secondary vortices are formed in the right top and left bottom corners. When the Rayleigh number increases, the size of secondary vortices also increases due to increasing magnitude of flow velocity.

Similar to the case of $k = 0.1$, the isotherms at $Ra = 10^3$ for $k = 50$ show top–bottom and left–right reflectional symmetries about the horizontal and vertical mid-planes and satisfy Eq. (4). The streamlines and isotherms circulating in the counter-clockwise direction at $Ra = 10^4$, 10^5 and 10^6 for $k = 50$ are diagonally symmetric and satisfy Eq. (5), similar to the case of $k = 0.1$. The

streamlines and isotherms at $Ra = 10^3$–10^6 for the cases of $k = 0.1$, $k = 50$ and neutral body reach the steady state after the initial transients, unlike the time-dependent flow and temperature fields at $Ra = 10^6$ for the case of adiabatic body.

If $k = 0.1$ at $Ra = 10^3$, the temperature gradients within the conducting body are significant as shown in Fig. 4(a). Thus the isotherms on the bottom hot wall show the ascending curve when we move from right or left wall to the center and as a result the temperature at the center in the lower part of enclosure is larger than that at the right and left corners. This temperature distribution gives the value less than 1 for the surface-averaged Nusselt number at the bottom hot wall at $Ra = 10^3$ for $k = 0.1$, as shown in Table 2. However, if k is increased to 50, the temperature in the conducting body is uniform and close to 0.5. Thus the isotherms on the bottom hot wall show the descending curve when we move from right or left wall to the center and as a result the temperature at the center in the lower part of enclosure is smaller than that at the right and left corners. The temperature gradients on the hot wall for $k = 50$ are larger than those for $k = 0.1$. Thus the value of surface-averaged Nusselt number at the bottom hot wall at $Ra = 10^3$ for $k = 50$ is larger than 1. When the Rayleigh numer increases to 10^4, the convection starts to play some role in heat transfer. The different temperature distribution in the conducting body for different k makes the isotherms for $k = 0.1$ rotate further in the counter-clockwise direction, compared to the case of $k = 50$. Thus the surface-averaged Nusselt number for $k = 50$ is less than that for $k = 0.1$ when $Ra = 10^4$, unlike the increasing surface-averaged Nusselt number with increasing k when $Ra = 10^3$. When the Rayleigh number increases further to 10^5 and 10^6, the fluid flow and heat transfer are mainly governed by convection and become less dependent on the temperature distribution in the conducting body for both cases of $k = 0.1$ and 50. Thus the surface-averaged Nusselt numbers for the case of $k = 50$ at $Ra = 10^5$ and 10^6 have the similar values to those for the case of $k = 0.1$, as shown in Table 2. Because the fluid flow and temperature fields for the case of $k = 50$ at $Ra = 10^3$–10^6 are similar to those for the case of neutral body, the values of surface-averaged Nusselt number for $k = 50$ are close to those for the case of neutral body.

Fig. 6 shows isotherms and streamlines in the enclosure for different Rayleigh numbers with heat-conducting body at $k = 1$ and $\alpha = 1$. Fig. 6 also shows the results for the case of pure Rayleigh–Bénard convection without a body in the horizontal enclosure in order to compare its results with the present ones. When $k = 1$, a thermal conductivity of fluid is equal to that of fluid. When $Ra = 10^3$ for $k = 1$, the isotherms are parallel to the horizontal walls, which are identical to the pure Rayleigh–Bénard convection and different from the cases of $k = 0.1$ and $k = 50$. As a result, the surface-averaged Nusselt number on the bottom hot wall for the case of $k = 1$ is equal to that for the case of pure Rayleigh–Bénard convection, larger than that for $k = 0.1$ and smaller than that for $k = 50$, as shown in Table 2. When the Rayleigh number increases to 10^4, the streamlines and isotherms for $k = 1$ circulate in the counter-clockwise direction, similar to those for the cases of $k = 0.1$ and $k = 50$. The temperature gradients in the conducting body for $k = 1$ are smaller than those for $k = 0.1$ and larger than those for $k = 50$. This distribution of isotherms in the conducting body makes the isotherms for $k = 1$ circulate in the counter-clockwise direction less than those for $k = 0.1$ and more than those for $k = 50$. As a result, the temperature gradients and corresponding surface-averaged Nusselt number on the bottom hot wall for the case of $k = 1$ are less than those for $k = 0.1$ and larger than those for $k = 50$. The variation of surface-averaged Nusselt number on the hot wall for different values of k when $Ra = 10^4$ is opposite to that when $Ra = 10^3$. With increasing k, the surface-averaged Nusselt number on the hot wall increases when $Ra = 10^3$ and decreases when $Ra = 10^4$. When the Rayleigh number increases further to 10^5 and 10^6, the distribution of streamlines and isotherms for the case of $k = 1$ is similar to those for the cases of $k = 0.1$ and $k = 50$. Thus the surface-averaged Nusselt number on the bottom hot wall for $k = 1$ is also similar to that for $k = 0.1$ and $k = 50$ when $Ra = 10^5$ and 10^6, as shown in Table 2. Because the temperature distribution for $k = 1$ is generally similar to that for the pure Rayleigh–Bénard convection except the central region of enclosure, the difference in the surface-averaged Nusselt number on the hot wall between the case of $k = 1$ and pure Rayleigh–Bénard convection is little.

Because the fluid flow does not exist or the magnitude of flow velocity is very small when $Ra = 10^3$ and 10^4, the predominant mode of heat transfer is conduction and the temperature distribution in the enclosure depends strongly on the thermal condition of a body. Thus the presence of a body with different thermal conditions such as adiabatic, isothermal and conducting body gives different values of surface-averaged Nusselt numbers and heat transfer on the bottom hot wall when $Ra = 10^3$ and 10^4. However, when the Rayleigh number increases to 10^5 and 10^6, the effect of convection on the fluid flow and heat transfer in the enclosure increases. Thus the temperature distribution in the enclosure and surface-averaged Nusselt number on the bottom hot wall for all the cases with a body at the center do not depend much on the thermal conditions of a body, except the case of adiabatic body in which the fluid flow and heat transfer are time-dependent.

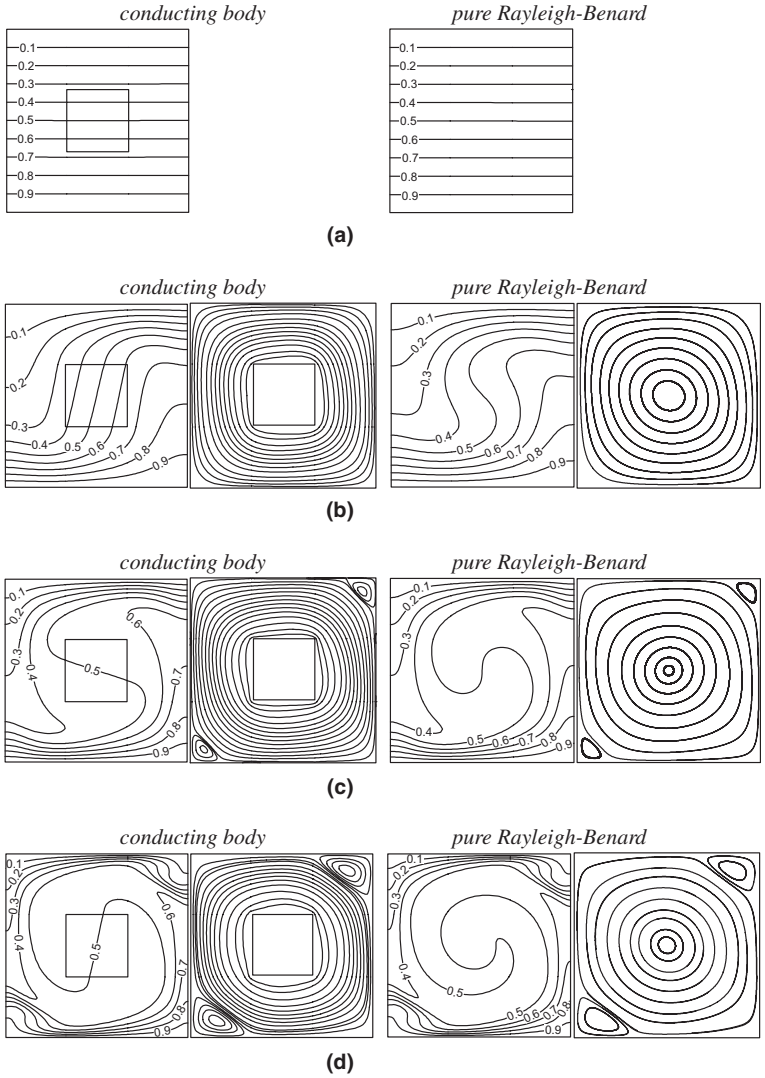

Fig. 6. Distribution of isotherms and streamline for the conducting body at $k = 1$ and $\alpha = 1$, and for the pure Rayleigh–Bénard convection for different Rayleigh numbers : (a) $Ra = 10^3$; (b) $Ra = 10^4$; (c) $Ra = 10^5$; (d) $Ra = 10^6$.

Fig. 7 shows the distribution of local Nusselt number along the bottom hot wall for different Rayleigh numbers and thermal conductivity ratios. When $Ra = 10^3$, the local Nusselt number is less than 1 when $k = 0.1$, parallel to the horizontal axis with a value of 1 when $k = 1$ and larger than 1 when $k = 50$. Because the heat transfer occurs mainly due to conduction and the isotherms are symmetric about $x = 0.5$, the local Nusselt number has the maximum and minimum values at the central position of $x = 0.5$ for both cases of $k = 0.1$ and $k = 50$ at the Rayleigh number of 10^3. When the Rayleigh number increases to 10^4, 10^5 and 10^6, the streamlines and isotherms circulate in the counter-clockwise direction and the location for the maximum local Nusselt number moves from the left wall to the center line. When $Ra = 10^4$, the local Nusselt number has a maximum value at the positions of $x_1 = 0.25$ for $k = 0.1$, $x_1 = 0.23$ for $k = 1$ and $x_1 = 0.18$ for $k = 50$, respectively. However, when the Rayleigh number increases to 10^6, the location x_3 for the maximum local Nusselt number is independent of the variation of thermal conductivity ratio and has a value of $x_3 = 0.34$. This result shows that the fluid flow and heat transfer at the lower Rayleigh number of 10^4 are affected by the variation of thermal conductivity ratio, but those at the higher Rayleigh number of 10^6 are almost independent of the thermal conductivity ratio. The local Nusselt number increases with increasing Rayleigh number as shown in Fig. 7.

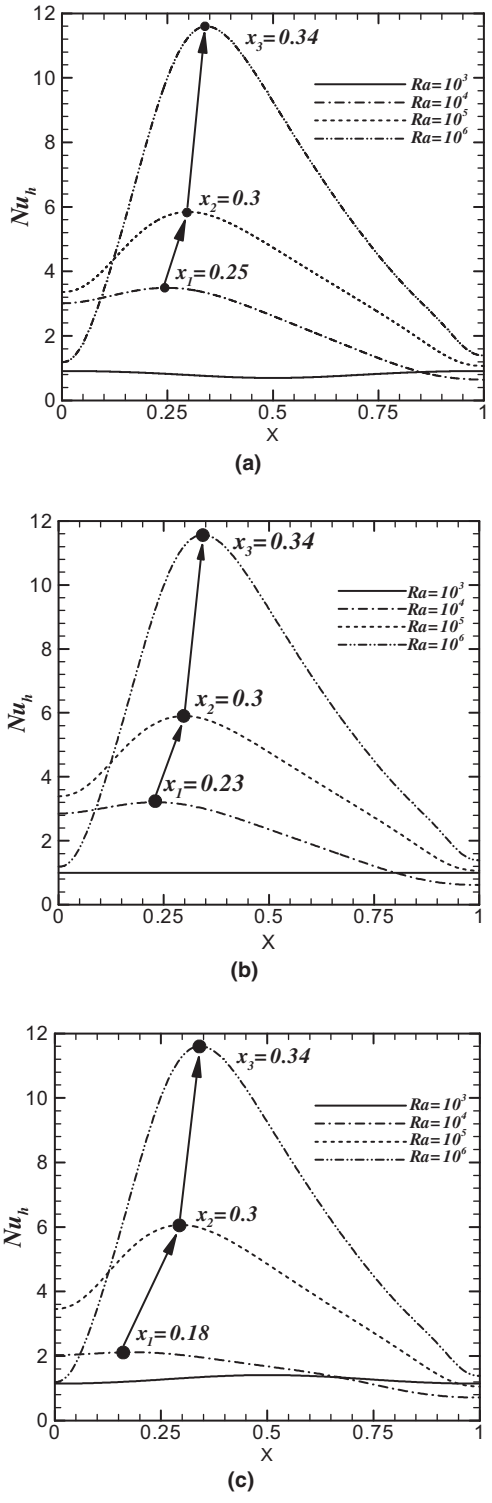

Fig. 7. Distribution of the local Nusselt number along the hot wall for different Rayleigh numbers and thermal conductivity ratios: (a) $k = 0.1$; (b) $k = 1$; (c) $k = 50$.

4. Conclusion

We have investigated natural convection in horizontal layer of fluid with a conducting body in the interior, using an accurate and efficient Chebyshev spectral collocation approach. A multi-domain methodology was employed to address the geometric complexity introduced by the internal body. We make a detailed analysis for the distribution of streamlines, isotherms and Nusselt number in order to investigate the effect of the presence of a conducting body on the fluid flow and heat transfer in the horizontal enclosure for the Rayleigh numbers in the range of $10^3 \leqslant Ra \leqslant 10^6$.

The fluid flow and corresponding heat transfer in the enclosure for $k = 0.1$, 1 and 50 are generally similar to those for the cases of adiabatic and neutral body and pure Rayleigh–Bénard convection, respectively, except the central region where the body exists.

When the Rayleigh number is less than 10^4, the effect of convection on the fluid flow and corresponding heat transfer is relatively weak and as a result the Nusselt number on the bottom hot wall depends on the variation of thermal conductivity ratio. However, when the Rayleigh number is larger than 10^5, the effect of convection becomes more dominant than conduction and as a result the Nusselt number on the bottom hot wall does not depend much on the variation of thermal conductivity ratio.

Acknowledgement

This work was partially supported by KOSEF.

References

[1] P.G. Drazin, W.H. Reid, Hydrodynamic Stability, Cambridge University Press, 1981, Chapter 2.
[2] F.B. Lipps, Numerical simulation of three-dimensional Bénard convection in air, J. Fluid Mech. 75 (1976) 113–148.
[3] S. Balachandar, M.R. Maxey, L. Sirovich, Numerical simulation of high Rayleigh number convection, J. Sci. Comput. 4 (1988) 219–236.
[4] G.D. Mallinson, G. de Vahl Davis, Three-dimensional natural convection in a box: a numerical study, J. Fluid Mech. 83 (1977) 1–31.
[5] T. Fusegi, J.M. Hyun, K. Kuwahara, B. Farouk, A numerical study of three-dimensional natural convection in a differentially heated cubical enclosure, Int. J. Heat Mass Transfer 34 (1991) 1543–1557.
[6] R.A.W. Henkes, C.J. Hoogendoorn, Scaling of turbulent natural convection flow in a heated square cavity, ASME J. Heat Transfer 116 (1994) 400–408.
[7] J.M. House, C. Beckermann, T.F. Smith, Effect of a centered conducting body on natural convection heat

transfer in an enclosure, Numer. Heat Transfer, Part. A 18 (1990) 213–225.
[8] J.Y. Oh, M.Y. Ha, K.C. Kim, Numerical study of heat transfer and flow of natural convection in an enclosure with a heat-generating conducting body, Numer. Heat Transfer, Part. A 31 (1997) 289–303.
[9] M.Y. Ha, M.J. Jung, Y.S. Kim, Numerical study on transient heat transfer and fluid flow of natural convection in an enclosure with a heat-generating conducting body, Numer. Heat Transfer, Part A 35 (1999) 415–433.
[10] M.Y. Ha, M.J. Jung, A numerical study on three-dimensional conjugate heat transfer of natural convection and conduction in a differentially heated cubic enclosure with a heat-generating cubic conducting body, Int. J. Heat Mass Transfer 43 (2000) 4229–4248.
[11] M.Y. Ha, H.S. Yoon, K.S. Yoon, S. Balachandar, I. Kim, J.R. Lee, H.H. Chun, Two-dimensional and unsteady natural convection in a horizontal enclosure with a square body, Numer. Heat Transfer, Part. A 41 (2002) 183–210.
[12] J.R. Lee, M.Y. Ha, S. Balachandar, H.S. Yoon, S.S. Lee, Natural convection in a horizontal layer of fluid with a periodic array of square cylinders in the interior, Phys. Fluids 16 (4) (2004) 1097–1117.
[13] C. Canuto, M.Y. Hussaini, A. Quarteroni, T.A. Zang, Spectral Methods in Fluid Dynamics, Springer Verlag, New York, 1988.
[14] G. de Vahl Davis, Natural convection of air in a square cavity: a benchmark numerical solution, Int. J. Numer. Methods Fluids 3 (1983) 249–264.
[15] P. Le Quere, Accurate solution to the square thermally driven cavity at high Rayleigh number, Comput. Fluids 20 (1991) 29.